

Continuous Mixtures of Tractable Probabilistic Models

Alvaro H.C. Correia^{1*}, Gennaro Gala^{1*}
Erik Quaeghebeur¹, Cassio de Campos¹, Robert Peharz^{1,2}

¹ Eindhoven University of Technology

² Graz University of Technology

{a.h.chaim.correia, g.gala, e.quaeghebeur, c.decampos, r.peharz}@tue.nl

Abstract

Probabilistic models based on continuous latent spaces, such as variational autoencoders, can be understood as uncountable mixture models where components depend continuously on the latent code. They have proven expressive tools for generative and probabilistic modelling, but are at odds with tractable probabilistic inference, that is, computing marginals and conditionals of the represented probability distribution. Meanwhile, tractable probabilistic models such as probabilistic circuits (PCs) can be understood as hierarchical discrete mixture models, which allows them to perform exact inference, but often they show subpar performance in comparison to continuous latent-space models. In this paper, we investigate a hybrid approach, namely continuous mixtures of tractable models with a small latent dimension. While these models are analytically intractable, they are well amenable to numerical integration schemes based on a finite set of integration points. With a large enough number of integration points the approximation becomes de-facto exact. Moreover, using a finite set of integration points, the approximation method can be compiled into a PC performing ‘exact inference in an approximate model’. In experiments, we show that this simple scheme proves remarkably effective, as PCs learned this way set new state-of-the-art for tractable models on many standard density estimation benchmarks.

Probabilistic modelling aims to capture the data-generating joint distribution, in order to subsequently perform probabilistic inference to answer queries of interest. A recurring scheme in probabilistic modelling is the use of an *uncountable mixture model*, that is, the data generating distribution is approximated by

$$p(\mathbf{x}) = \mathbb{E}_{p(\mathbf{z})} [p(\mathbf{x} | \mathbf{z})] = \int p(\mathbf{x} | \mathbf{z}) p(\mathbf{z}) d\mathbf{z} \quad (1)$$

where $p(\mathbf{z})$ is a mixing distribution (prior) over latent variables \mathbf{Z} , $p(\mathbf{x} | \mathbf{z})$ is a conditional distribution of \mathbf{x} given \mathbf{z} (mixture components), and $p(\mathbf{x})$ is the modelled density over variables \mathbf{X} , given by marginalising \mathbf{Z} from the joint $p(\mathbf{x} | \mathbf{z}) p(\mathbf{z})$.

Some successful recent examples of uncountable mixtures are variational autoencoders (VAEs) (Kingma and Welling 2013), generative adversarial networks (GANs) (Goodfellow et al. 2014), and normalising Flows (Rezende and Mohamed

2015). All three of these models use a simple prior $p(\mathbf{z})$, e.g. an isotropic Gaussian, and represent the mixture components with a neural network. In the case of VAEs, the mixture component is a proper density $p(\mathbf{x} | \mathbf{z})$ w.r.t. Lebesgue measure, represented by the so-called decoder, while for GANs and Flows the mixture component is a point measure, i.e., a deterministic function $\mathbf{x} = f(\mathbf{z})$.¹ The use of continuous neural networks topologically relates the latent space and the observable space with each other, so that these models can be described as *continuous* mixture models. The use of continuous mixtures allows to a certain extent the interpretation of \mathbf{Z} as a (latent) embedding of \mathbf{X} , but also seems to be beneficial for generalisation, i.e. to faithfully approximate real-world distributions with rather little training data.

However, while continuous mixture models have shown impressive results in density estimation and generative modelling, their ability to perform probabilistic inference remains rather limited. In particular, the key inference routines of *marginalisation and conditioning*, which together form a consistent reasoning process (Ghahramani 2015; Jaynes 2003), are generally intractable in these models, mainly due to the integral in (1) which forms a hard computational problem in general.

Meanwhile, the area of *tractable probabilistic modelling* aims for models which allow a wide range of exact and efficient inference routines. One of the most prominent frameworks to express tractable models are *probabilistic circuits* (PCs) (Vergari et al. 2020), which are computational graphs composed of (simple) tractable input distributions, factorisations (product nodes) and discrete mixture distributions (sum nodes). PCs describe many tractable models such as *Chow-Liu trees* (Chow and Liu 1968), *arithmetic circuits* (Darwiche 2003), *sum-product networks* (Poon and Domingos 2011), *cutset networks* (Rahman, Kothalkar, and Gogate 2014), *probabilistic sentential decision diagrams* (Kisa et al. 2014), and *generative forests* (Correia, Peharz, and de Campos 2020). The distribution represented by a PC depends both on its network structure and its parameters ϕ , which contains all sum weights and parameters for the PC’s input distributions.

From a representational point of view, PCs can be interpreted as hierarchical, discrete mixture models (Peharz et al.

*These authors contributed equally.

¹Moreover, for Flows the vectors \mathbf{z} and \mathbf{x} depend via a bijection on each other, so \mathbf{z} is not “really latent.”

2016; Zhao, Poupart, and Gordon 2016), i.e. they can be generally written as

$$p(\mathbf{x}) = \sum_{\mathbf{z}'} p(\mathbf{x} | \mathbf{z}') p(\mathbf{z}') \quad (2)$$

where \mathbf{Z}' is a *discrete* latent vector, but otherwise the form is similar to the continuous mixture in (1). The number of states of \mathbf{Z}' and thus the number of represented mixture components $p(\mathbf{x} | \mathbf{z}')$ grows exponentially in the depth of the PC (Peharz 2015; Zhao, Poupart, and Gordon 2016). Moreover, recent vectorisation-based implementations (Peharz et al. 2020a) allow to scale PCs to large sizes ($>100\text{M}$ of parameters) at execution speeds comparable to standard neural networks. These endeavours evidently boosted the performance of tractable models, yet there is still a significant gap to intractable models such as VAEs. One reason for this performance gap is likely the structural constraints in PCs, which are required to maintain tractability but are at odds with expressivity. On the other hand, a *huge* discrete mixture model of the form (2) should in principle be able to outperform moderately sized uncountable mixture (1). Yet, on vanilla benchmarks, we do not see this result; e.g. a vanilla VAE with a few million parameters easily gets test log-likelihoods higher than -90 nats on binary MNIST (Tomczak and Welling 2018), whereas an Einet with 84 million parameters (Peharz et al. 2020a) barely gets above -100 nats (see Table 3). Thus, a complementary explanation is that discrete (and hierarchical) mixtures—like PCs—are hard to learn (or generalise poorly), while continuous mixtures—like VAEs—are easier to learn (or generalise well).

In this paper, we follow a hybrid approach and consider *continuous mixtures of tractable models*. In particular, we consider continuous mixtures of two very simple tractable models, namely *completely factorised distributions* and *tree-shaped graphical models*, which can both be easily expressed as PCs. Specifically, we consider models of the form

$$p(\mathbf{x}) = \mathbb{E}_{p(\mathbf{z})} [p(\mathbf{x} | \phi(\mathbf{z}))] \quad (3)$$

where $p(\mathbf{z})$ is an isotropic Gaussian prior and $p(\mathbf{x} | \phi(\mathbf{z}))$ is a PC with its parameters depending on \mathbf{z} via some neural-network $\phi(\mathbf{z})$, similarly as in *Conditional SPNs* (Shao et al. 2020) and *HyperSPNs* (Shih, Sadigh, and Ermon 2021). While these models are analytically intractable, we can approximate the marginalisation of \mathbf{z} arbitrarily well with numerical techniques, such as *Gaussian quadrature rules* and *(quasi) Monte Carlo*. The common principle of these methods is that they select a finite set of *integration points* $\mathbf{z}_1, \dots, \mathbf{z}_N$ in either a deterministic or (partially) random manner and construct corresponding weight function $w(\mathbf{z})$ such that (3) is approximated as

$$p(\mathbf{x}) = \mathbb{E}_{p(\mathbf{z})} [p(\mathbf{x} | \phi(\mathbf{z}))] \approx \sum_{i=1}^N w(\mathbf{z}_i) p(\mathbf{x} | \phi(\mathbf{z}_i)). \quad (4)$$

All considered integration methods become exact for $N \rightarrow \infty$ and, under certain conditions on $\phi(\mathbf{z})$, one can derive guarantees for the approximation error for $N < \infty$. In particular, for (quasi) Monte Carlo integration it is straightforward to derive

probabilistic error guarantees for the approximation quality by leveraging concentration bounds. Moreover, an empirical observation is that numerical integration works reasonably well for low dimensional spaces, but tends to deteriorate for larger dimensionality. Thus, in this paper we keep the dimensionality of \mathbf{Z} small (≤ 20), so that our continuous mixtures of tractable models remain “morally tractable.”

Specifically, the integration weights $\{w(\mathbf{z}_i)\}_{i=1}^N$ sum to one,² so that the approximation in (4) can be interpreted as a discrete mixture model. For fixed \mathbf{z}_i , each $p(\mathbf{x} | \phi(\mathbf{z}_i))$ is simply a PC with fixed parameters $\phi_i = \phi(\mathbf{z}_i)$, so that (4) is in fact a mixture of PCs, which in turn can be again be interpreted as a larger PC (Vergari et al. 2020). Thus, we can convert a learned intractable model from (3) into a PC which facilitates exact inference, that is, “performing exact inference in an approximate model.”

To the best of our knowledge, this simple idea to construct tractable models has not been explored, yet it delivers astonishing results: On 16 out of 20 commonly used density estimation benchmarks, we set new state of the art in the domain of tractable models, outperforming even the most sophisticated PC structure and parameter learners. We also achieve competitive results on image datasets, and while not outperforming other PCs in terms of test log-likelihood, produce clearly better samples.

1 Background and Related Work

In this paper we are interested in *tractable* probabilistic models, i.e. models which allow exact and efficient inference. *Probabilistic circuits* (PCs) are a prominent language for tractable models and are defined as follows.

Definition 1 (Probabilistic Circuit). *Given a set of random variables \mathbf{X} , a probabilistic circuit (PC) is based on an acyclic directed graph \mathcal{S} containing three types of nodes: tractable distribution nodes over a subset of the random variables in \mathbf{X} , e.g. Gaussian, Categorical, or other exponential families; sum nodes, which compute a convex combination (a mixture) of their inputs; and product nodes, which compute the product (a factorisation) of their inputs. All leaves of \mathcal{S} are distribution nodes and all internal nodes are either sum or product nodes. We assume that \mathcal{S} has a single root, which is the output of the PC, computing a density over \mathbf{X} .*

As mentioned in the introduction, PCs can express many different tractable models (Vergari et al. 2020). Of particular interest in this paper will be PCs representing *completely factorised* distributions, i.e. $\mathcal{S} = \prod_{d=1}^D p(X_d)$, and *tree-shaped graphical models*, also called *Chow-Liu trees* (CLTs) (Chow and Liu 1968), which can be easily converted into PCs (Dang, Vergari, and Broeck 2020; Di Mauro et al. 2021). We will denote PC structures corresponding to factorised distributions as \mathcal{S}_F and CLT structures as \mathcal{S}_{CLT} . In order to obtain a suitable CLT in the first place, we will use the poly-time structure learner in (Chow and Liu 1968). While these structures

²For Monte Carlo, they are $w(\mathbf{z}_i) = \frac{1}{N}$. For Gaussian quadrature their sum might deviate from 1 for small N since $p(\mathbf{z})$ is non-polynomial. However, knowledge that $p(\mathbf{x})$ is a probability distribution gives licences to re-normalise the weights in this case.

are arguably simple, we will show in the experiment section that continuous mixtures of such PCs outperform all state-of-the-art PC learners on 16 out of 20 common benchmark datasets.

The perhaps most widely known *continuous mixture model* is the *variational autoencoder* (VAE) (Kingma and Welling 2013; Rezende and Mohamed 2015), specifying the model density as $p(\mathbf{x}) = \int p(\mathbf{x} | \phi(\mathbf{z})) p(\mathbf{z}) d\mathbf{z}$ where $p(\mathbf{z})$ is an isotropic Gaussian and $p(\mathbf{x} | \phi(\mathbf{z}))$ is typically a fully factorised distribution of Gaussians or Binomials, whose parameters are provided by a neural network $\phi(\mathbf{z})$ —the so-called decoder—taking \mathbf{z} as input. Since the latent code in VAEs is usually relatively high-dimensional, learning and inference is done via amortised inference (Kingma and Welling 2013).

When using \mathcal{S}_F , our models specify in fact the same model as VAEs, which has originally been introduced by McKay (MacKay 1995) under the name *density network*. Our work essentially re-visits McKay’s work, who already mentions: *For a hidden vector of sufficiently small dimensionality, a simple Monte Carlo approach to the evaluation of these integrals can be effective*. In this paper, we compare various numerical integration methods and find that randomised quasi Monte Carlo performs best for our purposes. Moreover, we use numerical approximation as a form of “*compilation approach*,” yielding an approximate tractable model and set new state of the art in the domain of tractable models.

Similar approaches to our method are HyperSPNs (Shih, Sadigh, and Ermon 2021) and conditional SPNs (Shao et al. 2020), which both use neural nets to compute the weights of PCs. However, HyperSPNs are primarily a regularisation technique that applies to a single PC, whereas in this work we use them to learn continuous mixtures of PCs. In conditional SPNs the parameters are a function of observed variables, while we use a continuous *latent* space in this work.

2 Inference and Learning

Our model as specified in (3) consists of a continuous latent space \mathbf{Z} and a given PC structure \mathcal{S} , whose parameters $\phi(\mathbf{z})$ are a differentiable function of the latent variables. We will broadly refer to function ϕ as *decoder* and to the model as whole as *continuous mixtures*. We use $\text{cm}(\mathcal{S}_F)$ and $\text{cm}(\mathcal{S}_{\text{CLT}})$ to denote continuous mixtures with factorised structure and CLT structure, respectively.

Amortised inference (Kingma and Welling 2013; Rezende and Mohamed 2015) is the de-facto standard way to learn continuous mixture models. In this approach, a separate neural network—the so-called *encoder*—represents an approximate posterior $q(\mathbf{z} | \mathbf{x})$. The encoder and decoder are learned simultaneously by maximizing the *evidence lower bound* (ELBO)

$$\mathbb{E}_q[\log p(\mathbf{x} | \mathbf{z}) - \log q(\mathbf{z} | \mathbf{x}) + \log p(\mathbf{z})] \quad (5)$$

which is a lower bound of the (marginal) log-likelihood $\log p(\mathbf{x})$ and thus a principled objective. At the same time, maximising the ELBO is moving q closer to the true posterior in Kullback-Leibler sense, hence tightening the ELBO.

In this paper, we investigate numerical integration as an alternative inference and learning method. In particular, we do not require an encoder or any other parametric form of approximate posterior.

2.1 Inference via Numerical Integration

Given some function f , a numerical integration method consists of a set of N integration points $\{\mathbf{z}_i\}_{i=1}^N$ and a weight function w such that the integration error $\varepsilon = \left| \int f(\mathbf{z}) d\mathbf{z} - \sum_{i=1}^N w(\mathbf{z}_i) f(\mathbf{z}_i) \right|$ is as small as possible. In this paper, we are interested in approximating the density $p(\mathbf{x}) = \int p(\mathbf{x} | \mathbf{z}) p(\mathbf{z}) d\mathbf{z}$ of a cm model, so that the integration error with integration points $\{\mathbf{z}_i\}_{i=1}^N$ is given as

$$\varepsilon_{\text{cm}}(\mathbf{x}, \{\mathbf{z}_i\}_{i=1}^N) = \left| \int p(\mathbf{x} | \phi(\mathbf{z})) p(\mathbf{z}) d\mathbf{z} - \sum_{i=1}^N w(\mathbf{z}_i) p(\mathbf{x} | \phi(\mathbf{z}_i)) \right|. \quad (6)$$

Quadrature Rules divide the integration domain into sub-intervals and approximate the integrand on these intervals with polynomials, which are easy to integrate. They yield a set of deterministic integration points and weights as a function of the degree of the interpolating polynomial. Common quadrature rules like trapezoidal and Simpson’s rule achieve error bounds of $\mathcal{O}(N^{-2})$ and $\mathcal{O}(N^{-4})$, respectively. *Gaussian quadrature rules* go a step further and take into account the distribution of \mathbf{z} , e.g. Gauss-Hermite quadrature is designed for indefinite integrals with $\mathbf{z} \sim \mathcal{N}(\mathbf{0}, \mathbf{1})$. They integrate exactly any polynomial of degree $2N-1$ or less, which makes them attractive for general integrands, since by the Weierstrass approximation theorem, any function can be approximated by a polynomial to arbitrary precision under mild regularity conditions.

Unfortunately, quadrature rules do not scale well to high dimensions, since multi-dimensional quadrature rules are usually constructed as the tensor product of univariate rules. If a univariate quadrature rule has an error bound of $\mathcal{O}(N^{-r})$, the corresponding rule in d dimensions with N^d integration points would achieve an error bound $\mathcal{O}(N^{-r/d})$, which degrades quickly due to the curse of dimensionality.

Sparse grids (Bungartz and Griebel 2004; Smolyak 1960) try to circumvent that by a special truncation of the tensor product expansion of univariate quadrature rules. This reduces the number of integration points to $\mathcal{O}(N(\log N)^{d-1})$ without significant drops in accuracy (Gerstner and Griebel 2010). However, even if the underlying quadrature formulas are positive, sparse grids can yield negative weights. In our preliminary experiments, this property of sparse grids was highly problematic, in particular when inference was used as part of a learning routine.

Monte Carlo (MC) methods cast the integral as an expectation such that we can compute $\int p(\mathbf{x} | \mathbf{z}) p(\mathbf{z}) d\mathbf{z}$ as $\mathbb{E}_{p(\mathbf{z})}[p(\mathbf{x} | \mathbf{z})] = \sum_{i=1}^N \frac{1}{N} p(\mathbf{x} | \mathbf{z}_i)$. MC is easy to use and especially attractive for high-dimensional problems since its convergence rate $\mathcal{O}(N^{-1/2})$ is independent of the problem dimensionality. However, this convergence rate decelerates quickly as one increases the number of integration points, which can be too slow. Quasi-Monte Carlo (QMC) methods (Caffisch 1998) replace a pseudo-random sequence of integration points with low-discrepancy sequences with the intent of reducing the variance in the MC estimator and converge faster than $\mathcal{O}(N^{-1/2})$. Crucially, QMC is determin-

istic, which makes it hard to estimate the integration error in practice. Randomised quasi-Monte Carlo (RQMC) reintroduces randomness into the low-discrepancy sequences of integration points, allowing for error estimation (via multiple simulations) and essentially turning QMC into a variance reduction method (l’Ecuyer 2016).

In our experiments, we opt for RQMC for mainly two reasons. First, its convergence does not depend directly on the dimensionality, meaning we have more freedom to choose the latent dimensionality. In fact, we empirically observe that increasing the latent dimensionality does not hurt performance (see additional results in Appendix B). We conjecture that training via numerical integration sufficiently regularises the decoder so that it remains amenable to numerical integration, even when using a relatively large latent dimensionality in the order of tens. Second, in contrast to Monte Carlo, it produces integration points of lower variance (l’Ecuyer 2016), which often facilitates training (see Appendix G), and, in comparison to QMC, reintroducing randomness into the sets of integration points helps avoiding overfitting.

2.2 Learning the Decoder

In principle, continuous mixture models can be learned in many ways, such as amortised inference (Kingma and Welling 2013) or adversarial training (Goodfellow et al. 2014). However, these methods do not encourage the decoder to be amenable to numerical integration, and thus their approximation by (or compilation to) a mixture of tractable models is subpar. Perhaps not surprisingly, we find that training via numerical integration is the best way to learn and extract expressive mixtures of tractable probabilistic models. We compare numerical integration and variational inference in Figure 1 and Appendix C.

Training via integration simply amounts to selecting a set of integration points $\{\mathbf{z}_i\}_{i=1}^N$ using any numerical integration method of choice and, for some training data $\{\mathbf{x}_j\}_{j=1}^M$, maximising the log-likelihood (LL) of the approximate model with respect to the decoder parameters:

$$LL = \sum_{j=1}^M \log \sum_{i=1}^N [w(\mathbf{z}_i) p(\mathbf{x}_j | \phi(\mathbf{z}_i))]. \quad (7)$$

For any integration method, when $N \rightarrow \infty$, this objective converges to the exact log-likelihood of the continuous mixture, and for $1 \ll N < \infty$ it serves as a reasonable approximation.

Specifically, when using (RQ)MC methods the inner sum of (7) is unbiased, yielding an *negatively biased* estimate of the true log-likelihood due to Jensen’s inequality—i.e. a “noisy lower bound”—justifying (7) as training objective for similar reasons as the variational ELBO (5). However, (7) should not be confused with the standard ELBO as it does not involve a posterior approximation and, unlike the ELBO, becomes tight for $N \rightarrow \infty$. We further note that (RQ)MC methods to estimate the log-likelihood of latent variable models is not a new idea and has been widely explored either directly (MacKay 1995) or to improve ELBO techniques (Burda, Grosse, and Salakhutdinov 2015; Mnih and Rezende 2016; Buchholz, Wenzel, and Mandt 2018). In this paper,

however, we are specifically interested in combining continuous mixtures with *tractable models* via numerical integration, as this direction has been explored rather little.

One can interpret our learned model in two distinct ways. The first is to interpret it as a “factory” method, whereby each fixed set of latent variables $\{\mathbf{z}_i\}_{i=1}^N$ yields a tractable model supporting exact likelihood and marginalisation, namely a PC (trivially a mixture of PCs is a PC). The second is to take it as an intractable continuous latent variable model, but one that is amenable to numerical integration. At test time, we are free to choose the set of integration points, possibly changing the integration method and number of integration points N if more or less precision is needed.

2.3 Latent Optimisation

As mentioned in the last section, once the decoder is trained, we can compile a continuous mixture into a PC by fixing a set of integration points selected by any integration method, leading to a discrete mixture of PCs. However, rather than using a fixed integration scheme, one might also treat the integration points as “parameters” and optimise them. Specifically, given training instances $\{\mathbf{x}_j\}_{j=1}^M$, we might find suitable $\{\mathbf{z}_i\}_{i=1}^N$ by maximising the log-likelihood:

$$\arg \max_{\{\mathbf{z}_i\}_{i=1}^N} \sum_{j=1}^M \log \sum_{i=1}^N w(\mathbf{z}_i) p(\mathbf{x}_j | \phi(\mathbf{z}_i)). \quad (8)$$

Due to the similarity to (Bojanowski et al. 2018; Park et al. 2019) we refer to this technique as *Latent Optimisation (LO)*, albeit some differences in spirit: In (Bojanowski et al. 2018; Park et al. 2019) the decoder and an individual latent representations for each training instance are jointly learned to minimise the reconstruction error. The latent space is regularised to follow a Gaussian prior, but otherwise is devoid of any probabilistic interpretation.

In our approach, however, the goal is an accurate yet compact approximation to the true continuous mixture model. Training the decoder and integration points together would lead to overfitting, meaning that the model would not translate well to different integration points or methods. For that reason, we only optimise the integration points as a *post-processing step*, i.e. the *decoder parameters remain fixed* throughout the optimisation process.

Our LO approach can also be interpreted as a way to learn (or compile) PCs, using continuous mixtures as a teacher model or regularizer. In our experiments, we see that this approach is remarkably effective. Specifically, LO yields the same test log-likelihoods as RQMC while using considerably fewer integration points, yielding compacter PCs.

3 Experiments

We evaluated our method on common benchmarks for generative models, namely 20 standard density estimation datasets as well as 4 image datasets (Binary-MNIST (Larochelle and Murray 2011), MNIST (LeCun et al. 1998), Fashion-MNIST (Xiao, Rasul, and Vollgraf 2017) and Street View House Numbers (SVHN) (Netzer et al. 2011)). All models were developed in python 3 with PyTorch (Paszke et al. 2019) and

Table 1: Average test log-likelihoods on 20 density estimation benchmarks. We compare $\text{cm}(\mathcal{S}_F)$, $\text{cm}(\mathcal{S}_{\text{CLT}})$ and $\text{LO}(\text{cm}(\mathcal{S}_{\text{CLT}}))$ with the best performance (BestPC) over 5 PC learning algorithms: Einet (Peharz et al. 2020a), LearnSPN (Gens and Pedro 2013), ID-SPN (Rooshenas and Lowd 2014), RAT-SPN (Peharz et al. 2020b) and HCLT (Liu and Van den Broeck 2021). We train using 2^{10} integration points and we sample 2^{13} mixture components from both $\text{cm}(\mathcal{S}_F)$ and $\text{cm}(\mathcal{S}_{\text{CLT}})$. LO is run over 2^{10} integration points. More complete results identifying each PC method are given in Table 10 in the Appendix. Higher is better.

Dataset	BestPC	$\text{cm}(\mathcal{S}_F)$	$\text{cm}(\mathcal{S}_{\text{CLT}})$	$\text{LO}(\text{cm}(\mathcal{S}_{\text{CLT}}))$	Dataset	BestPC	$\text{cm}(\mathcal{S}_F)$	$\text{cm}(\mathcal{S}_{\text{CLT}})$	$\text{LO}(\text{cm}(\mathcal{S}_{\text{CLT}}))$
accidents	-26.74	-33.27±0.03	-28.69±0.01	-28.81±0.02	jester	-52.46	-51.93±0.02	-51.94±0.01	-51.94±0.02
ad	-16.07	-18.71±0.15	-14.76±0.10	-14.42±0.09	kdd	-2.12	-2.13±0.00	-2.12±0.00	-2.12±0.00
baudio	-39.77	-39.02±0.02	-39.02±0.02	-39.04±0.02	kosarek	-10.60	-10.71±0.01	-10.56±0.01	-10.55±0.01
bbc	-248.33	-240.19±0.29	-242.83±0.55	-242.79±0.58	msnbc	-6.03	-6.14±0.01	-6.05±0.00	-6.05±0.00
bnetflix	-56.27	-55.49±0.02	-55.31±0.02	-55.36±0.02	msweb	-9.73	-9.68±0.00	-9.62±0.01	-9.60±0.01
book	-33.83	-33.67±0.04	-33.75±0.03	-33.55±0.02	nlts	-5.99	-5.99±0.00	-5.99±0.01	-5.99±0.00
c20ng	-151.47	-148.24±0.10	-148.17±0.09	-148.28±0.11	plants	-12.54	-12.45±0.02	-12.26±0.10	-12.27±0.01
cr52	-83.35	-81.52±0.08	-81.17±0.11	-81.31±0.15	pumbs	-22.40	-27.67±0.03	-23.71±0.03	-23.70±0.02
cwebkb	-151.84	-150.21±0.22	-147.77±0.26	-147.75±0.26	tmovie	-50.81	-48.69±0.09	-49.23±0.10	-49.29±0.12
dna	-79.05	-95.64±0.37	-84.91±0.09	-84.58±0.10	tretail	-10.84	10.85±0.00	-10.82±0.01	-10.81±0.01
Avg. rank	2.85	2.65	1.85	1.75					

trained with standard commercial GPUs. We used RQMC in all experiments ($w(\mathbf{z}_i) = 1/N$), with samples generated by QMCPy (Choi et al. 2020+).

3.1 Standard Density Estimation Benchmarks

As a first experiment, we compared *continuous mixtures of factorisations*, i.e. $\text{cm}(\mathcal{S}_F)$, and *continuous mixtures of CLTs*,³ i.e. $\text{cm}(\mathcal{S}_{\text{CLT}})$, as density estimators on a series of 20 standard commonly used benchmark datasets. In this set of experiments, we fixed the mixing distribution $p(\mathbf{z})$ to a 4-dimensional standard Gaussian.

We ran our models on each dataset using 5 different random seeds and trained for up to 200 epochs, with batch size 128, employing early stopping on the validation set with patience 15 to avoid overfitting. As decoders we used 6-layer MLPs with a progressively increasing number of units, LeakyReLUs activations, and batch normalisation layers (Ioffe and Szegedy 2015). For every optimisation step, we constructed a new set of integration points $\{\mathbf{z}_i\}_{i=1}^N$ from randomised lattice sequences of size $N = 2^{10}$. We then maximised the log-likelihood (7) using Adam (Kingma and Ba 2014). See Appendix A for comprehensive details.

At test time, the trained models can be evaluated with any number of integration points N , yielding a mixture of PCs and consequently indeed a standard PC (Vergari et al. 2020). Table 1 reports the test log-likelihoods for 2^{13} components,⁴ averaged over the 5 random seeds, and SOTA competitors. Our results set SOTA log-likelihoods for tractable models on 16 out of 20 datasets and are competitive on the remaining 4. For each dataset, we ranked the performance of the models involved from 1 to 4, and report the average rank at the bottom of the first half of the table. Particularly, we notice a substantial gap in performance between $\text{cm}(\mathcal{S}_{\text{CLT}})$ and $\text{cm}(\mathcal{S}_F)$

for the datasets accidents, ad, dna and pumbs, which are known to be highly structured. We want to stress that we used the same hyperparameters for all datasets, i.e. our SOTA results do not stem from extensive tuning efforts.

Figure 1 illustrates the effect of the number of integration points at test time, by plotting the performance of our models relative to the best results in Table 1, averaged over all 20 datasets. Note that $\text{cm}(\mathcal{S}_{\text{CLT}})$ generally outperforms $\text{cm}(\mathcal{S}_F)$ and the gap is accentuated when few integration points are used.

3.2 Latent Optimisation

Next, we showcase the effect of Latent Optimisation (LO), i.e. learning the integration points after having fit the decoder, as discussed in Section 2.3. Specifically, we run LO to search for a set of integration points for our trained $\text{cm}(\mathcal{S}_{\text{CLT}})$ by maximising (8) and show the results under $\text{LO}(\text{cm}(\mathcal{S}_{\text{CLT}}))$ in Table 1 and Figure 1.

We see that $\text{LO}(\text{cm}(\mathcal{S}_{\text{CLT}}))$ achieves essentially the same performance as $\text{cm}(\mathcal{S}_{\text{CLT}})$ but with *8 times fewer integration points*, leading to much smaller PCs. However, as can be seen in Figure 1, for a large number of integration points, (RQ)MC estimates already have low-variance and there is little room for improvement with LO. In fact, in this setting LO is prone to overfitting. This can be expected when the number of integration points becomes too large (in comparison to the training data), since they are treated as trainable parameters. For that reason, we limit our LO experiments to 2^{10} integration points in all datasets in Table 1 and 2.

3.3 Comparison with Variational Learning

As the main idea in this paper is connecting continuous mixtures with PCs via numerical integration, we used (7) so far to train our models. However, training a continuous mixture model and the conversion to a PC are orthogonal to each other, so we might also use traditional VAE training to learn continuous mixtures, i.e. maximising the ELBO (5) instead. In other words, we can train vanilla VAEs using a *small latent dimensionality* and convert the resulting models into PCs using RQMC or LO.

³CLT structures are learned using the classical algorithm (Chow and Liu 1968) and kept fixed during training.

⁴This was the largest number of components we used, which seemed sufficient for all datasets, as the results did not change further with more integration points. For some datasets, the continuous model is already approximated well with much smaller mixtures, see Appendix.

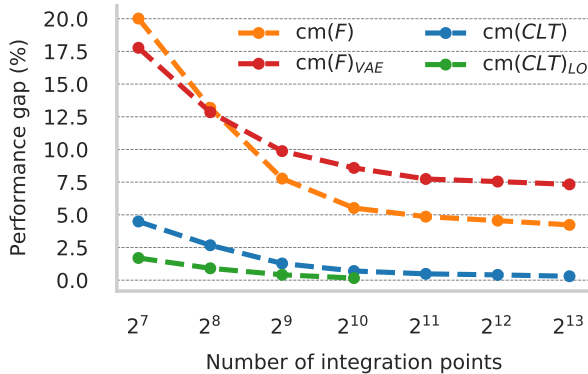


Figure 1: Relative performance gap to the best log-likelihood in Table 1 as a function of the number of integration points and averaged over all 20 datasets. Latent Optimisation is run (on purpose) for fewer number of integration points yet performs best. Lower is better.

For this purpose, we stuck to the same experimental setup for the 20 datasets and learned continuous mixtures with VAE training (Kingma and Welling 2013), denoted as $\text{cm}(\mathcal{S}_F^{\text{VAE}})$. Note that we used exactly the same architecture for both $\text{cm}(\mathcal{S}_F)$ and $\text{cm}(\mathcal{S}_F^{\text{VAE}})$, the only difference being the training objective.

Figure 1 shows that $\text{cm}(\mathcal{S}_F^{\text{VAE}})$ performs subpar to training via numerical integration, even with a large number of integration points at test time. There are two explanations for this result: First, it might be that the models $\text{cm}(\mathcal{S}_F^{\text{VAE}})$ are less amenable to our numerical approximation techniques and that the true log-likelihood is actually higher, or conversely, that models *trained* with numerical integration are also more amenable to numerical integration at test time. Second, it might also be that numerical integration leads to better model training for *small latent dimensionality*. We provide affirmative evidence for the latter in the Appendix.

However, evidently traditional VAE training is superior for large latent dimensionality, as numerical integration degrades quickly in high dimensional spaces. See the Appendix for more comprehensive experimental details and further results.

3.4 Binary-MNIST

We further evaluated our models on binary-MNIST (Larochelle and Murray 2011). We followed the same experimental protocol as in the previous experiments, except that we employed a larger latent dimensionality of 16 and therefore increase the number of integration points during training to 2^{14} . We did *not* use convolutions but rather stuck to the 6-layer MLP architecture scheme. We ran $\text{cm}(\mathcal{S}_F)$ and $\text{cm}(\mathcal{S}_{\text{CLT}})$ and applied LO to both final models for up to 50 epochs, using early stopping on the validation set to avoid overfitting. Table 2 shows that overall $\text{cm}(\mathcal{S}_{\text{CLT}})$ outperforms $\text{cm}(\mathcal{S}_F)$ and LO is remarkably effective when relatively few integration points are used.

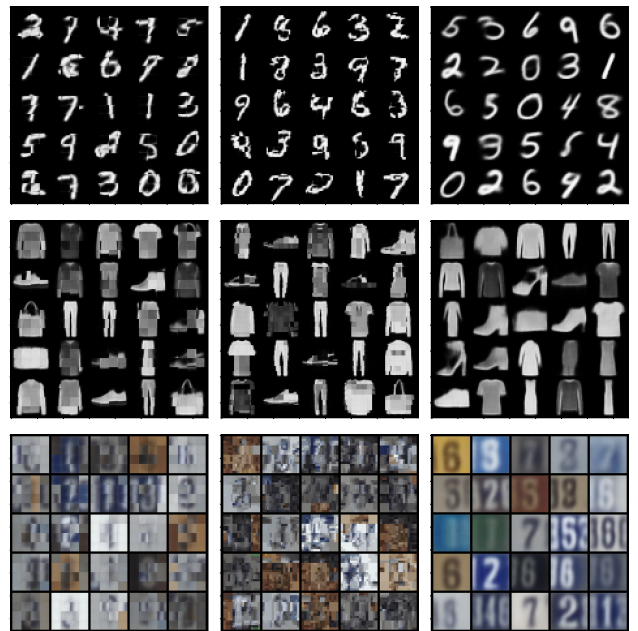


Figure 2: Samples from a small Einet with $\approx 5M$ parameters (left), a large Einet with $\approx 84M$ parameters (middle) and $\text{cm}(\mathcal{S}_F)$ with $\approx 100K$ parameters (right).

3.5 Image Datasets

We further evaluated our methods on (non-binary) image datasets. This time we use a convolutional architecture similar to that of DCGAN (Radford, Metz, and Chintala 2015), but we also included residual convolutional blocks as in (Van Den Oord, Vinyals et al. 2017). We compare against Einsum Networks (or EiNets) (Peharz et al. 2020a), large scale PCs specifically designed to take advantage of GPU accelerators. They are considered SOTA among tractable models for large unstructured data like images. For each dataset, we experimented with two different Einet structures with roughly 5 and 84 million parameters. Both architectures were defined via the Poon-Domingos structure scheme (Poon and Domingos 2011), recursively dividing the images in contiguous square blocks. For both EiNets and our model, pixels were modelled by a zero-mean normal distribution with constant standard deviation 0.1. No pre-processing step was taken. For all models, we fed the training data to the model without pre-clustering it into different components of the root sum node. Such a pre-processing step is applicable to any method and does not add to the analysis in this paper. That is why sample quality observed in Figure 2 is worse than as reported in (Peharz et al. 2020a), where images were clustered and a dedicated Einet was trained on each cluster.

As seen in Table 3, among the image datasets, we only outperform EiNets on binary-MNIST, when using Chow Liu Trees as leaves. That indicates that the structure in EiNets do help capture the underlying density in the datasets. However, an important caveat is that our models are extremely compact with the decoder given by a light convolutional architecture of approximately 100K parameters. That is orders

Table 2: Binary-MNIST test log-likelihoods for $\text{cm}(\mathcal{S}_F)$ and $\text{cm}(\mathcal{S}_{\text{CLT}})$ trained with 2^{14} integration points. In parentheses we report test log-likelihoods obtained via latent optimisation. Higher is better.

Model	N. Param	Number of integration points at test time							
		2^7	2^8	2^9	2^{10}	2^{11}	2^{12}	2^{13}	2^{14}
$\text{cm}(\mathcal{S}_F)$ (LO)	1.2M	-167.29 (-144.00)	-150.67 (-135.89)	-138.55 (-129.15)	-129.24 (-123.44)	-121.96	-116.42	-112.03	-108.69
$\text{cm}(\mathcal{S}_{\text{CLT}})$ (LO)	4.8M	-127.59 (-114.02)	-119.09 (-110.02)	-113.15 (-107.14)	-108.30 (-104.37)	-104.50	-101.55	-99.23	-97.48

Table 3: Test log-likelihoods on image data. Higher is better.

Model	Einet $\log p(\mathbf{x})$	Big Einet $\log p(\mathbf{x})$	Ours (2^{14}) $\log p(\mathbf{x})$
Binary-MNIST	-113.55	-99.82	-97.48
MNIST	284.63	668.19	235.48
Fashion-MNIST	418.24	645.30	412.01
SVHN	3080.35	3673.71	2807.95

of magnitude smaller than the competing EiNets, and still our model achieves very similar performance to the smallest of the EiNets which already had more than 5M parameters. Moreover, the higher log-likelihoods of EiNets come at the price of sample quality. In Figure 2, samples from $\text{cm}(\mathcal{S}_F)$ are clearly sharper and do not suffer from intense pixelation like those from EiNets. This is a clear manifestation of how good log-likelihoods and good sample quality are only weakly related (Theis, Oord, and Bethge 2015).

3.6 Other Tractable Queries

Our models also support efficient marginalisation, since the discrete approximation obtained via numerical integration is a PC in itself. That allows us to handle missing data and perform tasks like inpainting out-of-the-box, without any extra modelling steps. While this is not the focus of the paper—these queries are well-established for PCs, and it is not surprising that our models support them as well—we do present a couple of interesting experiments in Appendix F. We successfully trained our model on MNIST with substantially parts of the data missing. Note that such a training procedure is delicate for intractable models like VAEs. Furthermore, we included inpainting experiments on binary MNIST, MNIST and Fashion-MNIST, i.e. reconstructing missing data at test time, using a model trained on complete data.

4 Discussion

Our experiments demonstrate that continuous mixtures of PC—or actually their discrete approximations yielding again PCs—outperform most previous PC methods on several datasets. At first this might appear surprising, since for fixed N , a discrete mixture with N components is at least as expressive than a continuous mixture approximated by N integration points, since the former has mixture components with free (private) parameters, while the latter has components which are determined via a shared neural network and thus entangled in a complex way. Moreover, the PCs of previous works have been deeper and used more sophisticated architectures than our continuous mixtures (a comparison between

our models and the equivalent discrete mixtures is deferred to Appendix D, Table 6).

The main reason for the efficacy of our approach might be the continuity of the neural network, which topologically relates the latent and observable space, thus identifying some underlying latent structure—this is in fact one of the attractive and widely appreciated properties of VAEs. However, the effect of continuity on generalisation has not been much studied, and our results provide an interesting pointer in this regard.

Why does continuity promote generalisation, or act as some form of regularisation? For the one, there might be an Occam’s razor effect at work, since our models are usually much smaller in terms of parameters, yet they are expressive due to the non-linear nature of neural nets. Furthermore, dependence among components introduced via the latent space might effectively facilitate learning, by avoiding redundant or “dead” components, which have been observed in vanilla PCs (Dang, Liu, and Van den Broeck 2022).

These results have two important consequences for future work on tractable probabilistic models: (i) continuous latent spaces seem a valuable tool for learning tractable models and (ii) PCs in general seem to have untouched potential not yet exploited by existing learning methods.

5 Conclusion

In this paper, we have investigated the marriage of continuous mixtures and tractable probabilistic models. We have observed that even when using simple structures and standard numerical integration techniques, continuous latent variables facilitate the learning of expressive PCs, as confirmed by SOTA results on many datasets. Moreover, we have proposed latent optimisation as an effective way to derive competitive mixture models even with relatively few components (integration points). We believe this is a promising research avenue both in hybrid inference (Tan and Peharz 2019) and learning of tractable probabilistic models.

Our model is not without limitations, however. In particular, numerical integration is a computationally expensive training approach (the cost of each gradient update is proportional to the number of integration points), and we assume fixed PC structures (independent of the latent variables) that have to be defined or learned a-priori. Addressing these two issues are promising avenues for future work, especially with extensions to more complex structures, like HCLTs (Liu and Van den Broeck 2021) or even entire EiNets (Peharz et al. 2020a).

Authorship

A.H.C.C. and C.C. initially conceived the main idea, which was further developed and polished by all authors. All authors met regularly to discuss and to design the work. C.C. and R.P. supervised the project; E.Q. provided additional supervision of G.G.'s contribution. A.H.C.C. and G.G. developed the code and designed and performed the experiments. All authors analysed and checked results. All authors contributed to the final manuscript.

References

- Bojanowski, P.; Joulin, A.; Lopez-Pas, D.; and Szlam, A. 2018. Optimizing the Latent Space of Generative Networks. In *International Conference on Machine Learning*, 600–609. PMLR.
- Buchholz, A.; Wenzel, F.; and Mandt, S. 2018. Quasi-monte carlo variational inference. In *International Conference on Machine Learning*, 668–677. PMLR.
- Bungartz, H.-J.; and Griebel, M. 2004. Sparse grids. *Acta numerica*, 13: 147–269.
- Burda, Y.; Grosse, R.; and Salakhutdinov, R. 2015. Importance weighted autoencoders. *arXiv preprint arXiv:1509.00519*.
- Caffisch, R. E. 1998. Monte carlo and quasi-monte carlo methods. *Acta numerica*, 7: 1–49.
- Choi, S.-C. T.; Hickernell, F. J.; McCourt, M.; and Sorokin, A. 2020+. QMCPy: A quasi-Monte Carlo Python Library.
- Chow, C.; and Liu, C. 1968. Approximating discrete probability distributions with dependence trees. *IEEE transactions on Information Theory*, 14(3): 462–467.
- Correia, A.; Peharz, R.; and de Campos, C. P. 2020. Joints in Random Forests. *Advances in Neural Information Processing Systems*, 33.
- Dang, M.; Liu, A.; and Van den Broeck, G. 2022. Sparse Probabilistic Circuits via Pruning and Growing. In *The 5th Workshop on Tractable Probabilistic Modeling*.
- Dang, M.; Vergari, A.; and Broeck, G. V. d. 2020. Strudel: Learning Structured-Decomposable Probabilistic Circuits. *arXiv preprint arXiv:2007.09331*.
- Darwiche, A. 2003. A differential approach to inference in Bayesian networks. *Journal of the ACM (JACM)*, 50(3): 280–305.
- Di Mauro, N.; Gala, G.; Iannotta, M.; and Basile, T. M. 2021. Random probabilistic circuits. In *Uncertainty in Artificial Intelligence*, 1682–1691. PMLR.
- Gens, R.; and Pedro, D. 2013. Learning the structure of sum-product networks. In *International conference on machine learning*, 873–880. PMLR.
- Gerstner, T.; and Griebel, M. 2010. *Sparse Grids*. John Wiley & Sons, Ltd.
- Ghahramani, Z. 2015. Probabilistic machine learning and artificial intelligence. *Nature*, 521(7553): 452–459.
- Goodfellow, I. J.; Pouget-Abadie, J.; Mirza, M.; Xu, B.; Warde-Farley, D.; Ozair, S.; Courville, A. C.; and Bengio, Y. 2014. Generative Adversarial Nets. In *NIPS*.
- Ioffe, S.; and Szegedy, C. 2015. Batch normalization: Accelerating deep network training by reducing internal covariate shift. In *International conference on machine learning*, 448–456. PMLR.
- Jaynes, E. T. 2003. *Probability Theory: The Logic of Science*. Cambridge University Press.
- Kingma, D. P.; and Ba, J. 2014. Adam: A method for stochastic optimization. *arXiv preprint arXiv:1412.6980*.
- Kingma, D. P.; and Welling, M. 2013. Auto-encoding variational bayes. *arXiv preprint arXiv:1312.6114*.
- Kisa, D.; Van den Broeck, G.; Choi, A.; and Darwiche, A. 2014. Probabilistic sentential decision diagrams. In *Proceedings of the 14th international conference on principles of knowledge representation and reasoning (KR)*, 1–10.
- Larochelle, H.; and Murray, I. 2011. The neural autoregressive distribution estimator. In *Proceedings of the fourteenth international conference on artificial intelligence and statistics*, 29–37. JMLR Workshop and Conference Proceedings.
- LeCun, Y.; Bottou, L.; Bengio, Y.; and Haffner, P. 1998. Gradient-based learning applied to document recognition. *Proceedings of the IEEE*, 86(11): 2278–2324.
- Liang, Y.; Bekker, J.; and Van den Broeck, G. 2017. Learning the structure of probabilistic sentential decision diagrams. In *Proceedings of the 33rd Conference on Uncertainty in Artificial Intelligence (UAI)*.
- Liu, A.; and Van den Broeck, G. 2021. Tractable regularization of probabilistic circuits. *Advances in Neural Information Processing Systems*, 34.
- l’Ecuyer, P. 2016. Randomized quasi-Monte Carlo: An introduction for practitioners. In *International Conference on Monte Carlo and Quasi-Monte Carlo Methods in Scientific Computing*, 29–52. Springer.
- MacKay, D. J. 1995. Bayesian neural networks and density networks. *Nuclear Instruments and Methods in Physics Research Section A: Accelerators, Spectrometers, Detectors and Associated Equipment*, 354(1): 73–80.
- Mnih, A.; and Rezende, D. 2016. Variational inference for monte carlo objectives. In *International Conference on Machine Learning*, 2188–2196.
- Netzer, Y.; Wang, T.; Coates, A.; Bissacco, A.; Wu, B.; and Ng, A. Y. 2011. Reading digits in natural images with unsupervised feature learning.
- Park, J. J.; Florence, P.; Straub, J.; Newcombe, R.; and Lovegrove, S. 2019. DeepSDF: Learning continuous signed distance functions for shape representation. In *Proceedings of the IEEE/CVF conference on computer vision and pattern recognition*, 165–174.
- Paszke, A.; Gross, S.; Massa, F.; Lerer, A.; Bradbury, J.; Chanan, G.; Killeen, T.; Lin, Z.; Gimelshein, N.; Antiga, L.; et al. 2019. Pytorch: An imperative style, high-performance deep learning library. *arXiv preprint arXiv:1912.01703*.
- Peharz, R. 2015. *Foundations of Sum-Product Networks for Probabilistic Modeling*. Ph.D. thesis, Graz University of Technology.

- Peharz, R.; Gens, R.; Pernkopf, F.; and Domingos, P. 2016. On the latent variable interpretation in sum-product networks. *IEEE transactions on pattern analysis and machine intelligence*, 39(10): 2030–2044.
- Peharz, R.; Lang, S.; Vergari, A.; Stelzner, K.; Molina, A.; Trapp, M.; Van den Broeck, G.; Kersting, K.; and Ghahramani, Z. 2020a. Einsum networks: Fast and scalable learning of tractable probabilistic circuits. In *International Conference on Machine Learning*, 7563–7574. PMLR.
- Peharz, R.; Tschitschek, S.; Pernkopf, F.; and Domingos, P. 2015. On Theoretical Properties of Sum-Product Networks. In *Proceedings of AISTATS*, 744–752.
- Peharz, R.; Vergari, A.; Stelzner, K.; Molina, A.; Shao, X.; Trapp, M.; Kersting, K.; and Ghahramani, Z. 2020b. Random sum-product networks: A simple and effective approach to probabilistic deep learning. In *Uncertainty in Artificial Intelligence*, 334–344. PMLR.
- Poon, H.; and Domingos, P. 2011. Sum-product networks: A new deep architecture. In *2011 IEEE International Conference on Computer Vision Workshops (ICCV Workshops)*, 689–690. IEEE.
- Radford, A.; Metz, L.; and Chintala, S. 2015. Unsupervised representation learning with deep convolutional generative adversarial networks. *arXiv preprint arXiv:1511.06434*.
- Rahman, T.; Kothalkar, P.; and Gogate, V. 2014. Cutset networks: A simple, tractable, and scalable approach for improving the accuracy of Chow-Liu trees. In *Joint European conference on machine learning and knowledge discovery in databases*, 630–645. Springer.
- Rezende, D.; and Mohamed, S. 2015. Variational inference with normalizing flows. In *International conference on machine learning*, 1530–1538. PMLR.
- Rezende, D. J.; Mohamed, S.; and Wierstra, D. 2014. Stochastic backpropagation and approximate inference in deep generative models. In *International conference on machine learning*, 1278–1286. PMLR.
- Rooshenas, A.; and Lowd, D. 2014. Learning sum-product networks with direct and indirect variable interactions. In *International Conference on Machine Learning*, 710–718. PMLR.
- Shao, X.; Molina, A.; Vergari, A.; Stelzner, K.; Peharz, R.; Liebig, T.; and Kersting, K. 2020. Conditional sum-product networks: Imposing structure on deep probabilistic architectures. In *International Conference on Probabilistic Graphical Models*, 401–412. PMLR.
- Shih, A.; Sadigh, D.; and Ermon, S. 2021. HyperSPNs: Compact and Expressive Probabilistic Circuits. *Advances in Neural Information Processing Systems*, 34.
- Smolyak, S. A. 1960. Interpolation and quadrature formulas for the classes W_s^α and E_s^α . 131(5): 1028–1031.
- Tan, P. L.; and Peharz, R. 2019. Hierarchical Compositional Mixtures of Variational Autoencoders. In Chaudhuri, K.; and Salakhutdinov, R., eds., *Proceedings of the 36th International Conference on Machine Learning*, volume 97 of *Proceedings of Machine Learning Research*, 6115–6124. PMLR.
- Theis, L.; Oord, A. v. d.; and Bethge, M. 2015. A note on the evaluation of generative models. *arXiv preprint arXiv:1511.01844*.
- Tomczak, J.; and Welling, M. 2018. VAE with a VampPrior. In *International Conference on Artificial Intelligence and Statistics*, 1214–1223. PMLR.
- Van Den Oord, A.; Vinyals, O.; et al. 2017. Neural discrete representation learning. *Advances in neural information processing systems*, 30.
- Vergari, A.; Choi, Y.; Peharz, R.; and Van den Broeck, G. 2020. Probabilistic Circuits: Representations, Inference, Learning and Applications. <http://starai.cs.ucla.edu/slides/AAAI20.pdf>. Tutorial at AAAI 2020.
- Xiao, H.; Rasul, K.; and Vollgraf, R. 2017. Fashion-mnist: a novel image dataset for benchmarking machine learning algorithms. *arXiv preprint arXiv:1708.07747*.
- Zhao, H.; Poupart, P.; and Gordon, G. 2016. A unified approach for learning the parameters of sum-product networks. *arXiv preprint arXiv:1601.00318*.

A Model Description

A.1 Latent Space

We use $d=4$ latent variables for the 20 density estimation benchmarks, and $d=16$ for the image datasets (Binary-MNIST (Larochelle and Murray 2011), MNIST (LeCun et al. 1998), Fashion-MNIST (Xiao, Rasul, and Vollgraf 2017) and Street View House Numbers (SVHN) (Netzer et al. 2011)). In all cases, the latent space was distributed as a standard normal, $\mathbf{z} \sim \mathcal{N}(0, 1)^d$, and integration points $\{\mathbf{z}_{i=1}^N\}$ were generated via a low-discrepancy lattice sequence. In practice, quasi-Monte Carlo methods are designed for sequences $\{\mathbf{u}_{i=1}^N\}$ mimicking a uniform distribution $\mathcal{U}(0, 1)^d$. However, for most commonly used distributions, it is easy to map uniform samples to the random variable of interest. For instance, for \mathbf{z} distributed as a multivariate normal with mean μ and covariance Σ , we can construct a sequence $\{\mathbf{z}_{i=1}^N\}$ from $\{\mathbf{u}_{i=1}^N\}$ as

$$\mathbf{z}_i = \Phi^{-1}(\mathbf{u}_i)\Sigma^{1/2} + \mu, \quad (9)$$

where Φ^{-1} is the inverse CDF of a standard normal distribution.

We choose a standard normal prior to facilitate the comparison to plain Variational Autoencoders (Kingma and Welling 2013). We have experimented with other distributions in preliminary studies, especially $\mathcal{U}(0, 1)^d$, but have not observed significant differences in performance.

A.2 Decoder architecture

In all experiments, only two architectures were considered depending on the type of data. For binary datasets, the decoder was a multi-layer perceptron (MLP) with 6 layers of progressively increasing hidden size (from latent dimension to input dimension). For continuous datasets we used a convolutional architecture similar to that of DCGAN (Radford, Metz, and Chintala 2015), but we also included residual convolutional blocks as in (Van Den Oord, Vinyals et al. 2017). In all cases, we used LeakyReLU activations and batch normalisation.

A.3 Structure in Tractable Probabilistic Models

Our method consists of a continuous mixture of tractable probabilistic models. The parameters of these models are a function of the continuous latent variables, and thus learnt, but their structure is assumed and has to be defined a priori. As discussed in the main text, we consider two types of structure a fully factorised distribution \mathcal{S}_F and a Chow-Liu Tree \mathcal{S}_{CLT} , which is learnt a priori using the training data. Ultimately, both structures are a composition of univariate distributions. For all these models, we use Bernoulli distributions with learnable parameters for binary data, and normal distributions with learnable means for continuous data. In the latter, we keep the standard deviation fixed so that test log-likelihoods of different models remain comparable. We use $\sigma=0.1$ in all continuous data experiments. In the case of Einets (Peharz et al. 2020a), we use the publicly available implementation by Peharz et al. with the exact same leaf distributions as just described above, and train via EM.

A.4 Training

We train via numerical integration with Randomised quasi-Monte Carlo (RQMC). At each training step, we generate a new low-discrepancy lattice sequence via *random shifting*. That is, we generate a lattice sequence $\{\mathbf{u}_{i=1}^N\}$ in $(0, 1)^d$ and, at each iteration, we shift it by adding a single random point to all other points in the sequence modulo 1.

$$\{\mathbf{u}'_{i=1}^N\} = \{\mathbf{u}_{i=1}^N\} + \mathbf{u}_{shift}(\text{mod } 1), \quad \mathbf{u}_{shift} \sim \mathcal{U}(0, 1)^d. \quad (10)$$

After shifting, $\{\mathbf{u}_{i=1}^N\}$ is mapped to $\{\mathbf{z}_{i=1}^N\}$ via a suitable transformation as described above. This is the simplest form of randomisation in RQMC and works well in practice. We recommend (l’Ecuyer 2016) for a good overview of RQMC methods. We train all models (including $\text{cm}(\mathcal{S}_F^{\text{VAE}})$) for 300 epochs using Adam (Kingma and Ba 2014) with learning rate of $1e^{-3}$, $\beta_1=0.9$ and $\beta_2=0.999$. We also track performance on the validation set and use early-stopping with a patience of 15 to avoid overfitting. In the case of $\text{cm}(\mathcal{S}_F)$ and $\text{cm}(\mathcal{S}_{CLT})$, we use 2^{10} integration points for binary datasets, and 2^{14} for image datasets. We report results across 5 random seeds, which we set to $\{0, 1, 2, 3, 4\}$. At test time, RQMC sequences are still stochastic, so we evaluate models with random seed set to 42 for reproducibility.

B Effect of Latent Space Dimensionality

We also investigate the effect of the latent space dimensionality on the overall performance of the model. We trained a $\text{cm}(\mathcal{S}_F)$ on Binary-MNIST (Larochelle and Murray 2011) with different latent dimensions d , namely $d=2^i$ for $i \in \{0, 1, 2, 3, 4, 5, 6\}$. We train all models with 2^{14} integration points but vary the number of integration points at test time from 2^8 to 2^{16} , as shown in Figure 3. In the following discussion, when referring to integration points we mean those used at *test time*.

For low numbers of integration points (up to 1024), models with small latent spaces perform best. That is as expected, since small latent spaces are more amenable to numerical integration. However, as we increase the number of integration points, it is clear the model benefits from larger latent dimensions, eventually converging for 8 latent dimensions or higher. That is somewhat surprising, since numerical integration in high dimensions is notoriously difficult and we would expect performance to deteriorate as we increase the latent dimensionality. We hypothesise training via numerical integration strongly regularises the decoder so that the learned function is smooth enough to allow for reliable numerical integration irrespective of the latent dimensionality.

In Figure 3, we report the same analysis for cm models trained via variational inference, $\text{cm}(\mathcal{S}_F^{\text{VAE}})$. We use the same decoder architecture and training protocol (see Appendix A) as for $\text{cm}(\mathcal{S}_F)$. Here we do observe that numerical integration struggles with high latent spaces, as test log-likelihoods rapid decline for $d \geq 4$. That is simply because the numerical integration becomes harder, since the ELBO actually improves for higher latent dimensions as shown in Table 4.

In all cases, it seems easier to numerically integrate—or extract good mixtures of tractable models from—models

learned via numerical than models trained via variational inference. For $d \leq 4$, numerical integration outperforms variational inference, whereas for $d > 4$ we still get better mixtures from $\text{cm}(\mathcal{S}_F)$ than from $\text{cm}(\mathcal{S}_F^{\text{VAE}})$, although the latter is more expressive as indicated by the ELBO.

C Training via Amortised Variational Inference

In this section, we expand the discussion on (amortised) variational inference (Kingma and Welling 2013; Rezende, Mohamed, and Wierstra 2014) by considering binary density estimation benchmarks and limiting the latent dimensionality to 4. In Table 5 we report the results obtained using a $\text{cm}(\mathcal{S}_F^{\text{VAE}})$ with 4 latent dimensions and standard normal prior. For 11 out of the 20 datasets, we could not match the ELBO (computed with 1000 MC samples) even when integrating with 2^{13} points, which indicates variational inference induces a complex decoder that is not always amenable to numerical integration, even in relatively low dimensions. Moreover, in all but 3 datasets, a cm model trained via numerical integration ($\text{cm}(\mathcal{S}_F)$), outperformed $\text{cm}(\mathcal{S}_F^{\text{VAE}})$.

These results indicate numerical integration is the best method to learn continuous mixtures of tractable probabilistic models. However, amortised variational inference is probably the most popular way to train continuous latent variables models and is more efficient than numerical integration: for each data point \mathbf{x} , variational inference computes $p(\mathbf{x} | \phi(\mathbf{z}_i))$ for only a few samples \mathbf{z}_i from the posterior (as few as one (Kingma and Welling 2013)), whereas numerical integration has to compute it once for every integration point. Therefore, it would be interesting to be able to extract good mixtures from models learned via variational inference. We believe one can improve on this by sufficiently regularising the decoder (e.g. penalising high Lipschitz constants) and thus facilitating numerical integration, but we leave that for future research.

D Plain Mixture Models

For Monte Carlo integration with a fixed number of integration points N , the approximate model resembles a plain mixture model with equally-probable weights:

$$\begin{aligned}\hat{p}(\mathbf{x}) &= \frac{1}{N} \sum_{i=1}^N p(\mathbf{x} | \phi(\mathbf{z}_i)) \approx \\ p(\mathbf{x}) &= \int p(\mathbf{x} | \phi(\mathbf{z})) p(\mathbf{z}) d\mathbf{z}.\end{aligned}\quad (11)$$

Thus it makes sense to compare our models to plain mixture models. That is, instead of having mixture components as a function of some latent variable, each component p_i is fully independent with

$$p_{\text{mix}}(\mathbf{x}) = \frac{1}{N} \sum_{i=1}^N p_i(\mathbf{x}). \quad (12)$$

In Table 6, we compare plain mixtures to a $\text{cm}(\mathcal{S}_F)$ with 4 latent dimensions. We use a fully factorised structure for both

models, that is

$$p_i(\mathbf{x}) = \prod_{j=1}^{|\mathbf{x}|} p_i(x_j) \quad \text{for plain mixture models,} \quad (13)$$

$$p(\mathbf{x} | \phi(\mathbf{z}_i)) = \prod_{j=1}^{|\mathbf{x}|} p(x_j | \phi(\mathbf{z}_i)) \quad \text{for } \text{cm}(\mathcal{S}_F). \quad (14)$$

We train both models using the exact same protocol (see Appendix A). The results in Table 6 show that our model outperformed plain mixtures ($\text{dm}(\mathcal{S}_F)$) in all datasets, even though both models were trained the exact same way and have the exact same structure if we consider a $\text{cm}(\mathcal{S}_F)$ compiled to a 1024 components mixture. The only difference is how we parametrise the mixture components.

Similarly, we also considered mixture models with learnable weights, that is

$$p_i(\mathbf{x}) = \prod_{j=1}^{|\mathbf{x}|} w_i p_i(x_j), \quad (15)$$

where $\{w_i\}_{i=1}^N$ are learnable parameters. We train these mixture models both via gradient descent ($\text{dm}(\mathcal{S}_F^W)$) and Expectation Maximisation ($\text{dm}(\mathcal{S}_F^{EM})$). As shown in Table 6, our model outperforms plain mixtures in all datasets but `dna` and `msnbc`, where learning via EM produces better test log-likelihoods. However, existing PC architectures (namely HCLT and RAT-SPNs) already performed better than our models in these datasets, so it is not that surprising that a discrete mixture works well for these two datasets.

For a fixed number of integration points (mixture components) discrete mixture models are strictly more expressive than continuous ones, since the parameters of each component are completely independent. Yet, continuous mixtures outperform discrete ones in almost all cases, indicating the regularisation introduced by the shared ‘decoder’ does facilitate learning. This result, albeit not surprising, has never been fully exploited in the tractable probabilistic models literature, to the best of our knowledge.

E Additional Experimental Results

In this section, we present additional results on continuous mixtures, showing test log-likelihoods on the 20 binary density estimation benchmarks for different numbers of integration points in Tables 7 and 8. We also include latent optimisation results for $\text{cm}(\mathcal{S}_{\text{CLT}})$ in Table 9, showing significant improvements especially when using few integration points. The same trend can be observed in Figure 4, where we show the performance of $\text{cm}(\mathcal{S}_F)$, $\text{cm}(\mathcal{S}_{\text{CLT}})$, $\text{LO}(\text{cm}(\mathcal{S}_{\text{CLT}}))$ and $\text{cm}(\mathcal{S}_F^{\text{VAE}})$ for all 20 density estimation benchmarks for different numbers of integration points.

Table 6: Test log-likelihoods for plain mixtures with non-learnable equally-probable weights trained via gradient descent ($\text{dm}(\mathcal{S}_F)$), with learnable weights also trained via gradient descent ($\text{dm}(\mathcal{S}_F^W)$), with learnable weights trained via EM ($\text{dm}(\mathcal{S}_F^{EM})$), and $\text{cm}(\mathcal{S}_F)$ on 20 standard density estimation benchmarks. All models are trained for up to 300 epochs using early stopping and employing 1024 components. Higher is better.

Dataset	$\text{dm}(\mathcal{S}_F)$	$\text{dm}(\mathcal{S}_F^W)$	$\text{dm}(\mathcal{S}_F^{EM})$	$\text{cm}(\mathcal{S}_F)$	Dataset	$\text{dm}(\mathcal{S}_F)$	$\text{dm}(\mathcal{S}_F^W)$	$\text{dm}(\mathcal{S}_F^{EM})$	$\text{cm}(\mathcal{S}_F)$
accidents	-42.58	-40.61	-35.38	-33.94	jester	-55.32	-53.54	-52.54	-52.03
ad	-104.57	-97.79	-24.91	-20.42	kdd	-6.81	-2.15	-2.14	-2.13
baudio	-42.24	-40.41	-39.76	-39.14	kosarek	-16.20	-11.17	-10.88	-10.75
bbc	-281.88	-288.31	-252.82	-241.54	msnbc	-6.36	-6.12	-6.03	-6.15
bnetflix	-58.19	-57.00	-56.34	-55.71	msweb	-18.29	-11.36	-10.00	-9.72
book	-41.72	-35.61	-34.66	-33.79	nlcs	-6.16	-6.01	-6.00	-6.00
c20ng	-163.04	-157.80	-151.79	-149.10	plants	-16.66	-14.41	-13.44	-12.65
cr52	-104.91	-98.79	-87.07	-82.33	pumbs	-46.59	-42.90	-32.84	-28.50
cwebkb	-176.60	-170.90	-154.75	-151.00	tmovie	-66.94	-61.64	-52.80	-49.12
dna	-101.93	-98.14	-94.46	-96.11	tretail	-18.35	-11.42	-10.90	-10.85

Table 7: Average $\text{cm}(\mathcal{S}_F)$ test log-likelihoods across 5 random seeds. Higher is better

Dataset	Mix-2 ⁷	Mix-2 ⁸	Mix-2 ⁹	Mix-2 ¹⁰	Mix-2 ¹¹	Mix-2 ¹²	Mix-2 ¹³
accidents	-38.78±0.22	-36.62±0.17	-34.85±0.11	-33.94±0.05	-33.58±0.05	-33.41±0.05	-33.27±0.03
ad	-42.89±2.39	-32.50±1.44	-23.79±0.93	-20.42±0.14	-19.59±0.11	-19.18±0.10	-18.71±0.15
baudio	-40.24±0.07	-39.76±0.03	-39.34±0.01	-39.14±0.01	-39.07±0.01	-39.05±0.01	-39.02±0.01
bbc	-249.58±0.66	-245.66±0.68	-243.06±0.34	-241.54±0.31	-240.78±0.36	-240.53±0.32	-240.19±0.29
bnetflix	-57.35±0.09	-56.65±0.12	-56.02±0.01	-55.71±0.01	-55.58±0.01	-55.54±0.01	-55.49±0.02
book	-34.51±0.05	-34.16±0.03	-33.92±0.04	-33.79±0.04	-33.72±0.04	-33.69±0.04	-33.67±0.04
c20ng	-153.71±0.56	-151.58±0.45	-149.96±0.30	-149.10±0.21	-148.64±0.15	-148.45±0.12	-148.24±0.10
cr52	-87.57±0.64	-85.51±0.48	-83.35±0.37	-82.33±0.18	-81.93±0.13	-81.74±0.08	-81.52±0.08
cwebkb	-155.62±0.68	-153.70±0.43	-151.93±0.26	-151.00±0.17	-150.59±0.18	-150.43±0.21	-150.21±0.22
dna	-99.04±0.50	-97.80±0.17	-96.62±0.17	-96.11±0.25	-95.86±0.31	-95.77±0.33	-95.64±0.37
jester	-52.97±0.03	-52.53±0.04	-52.20±0.02	-52.03±0.01	-51.97±0.02	-51.95±0.02	-51.93±0.02
kdd	-2.20±0.03	-2.18±0.04	-2.15±0.01	-2.13±0.00	-2.13±0.00	-2.13±0.00	-2.13±0.00
kosarek	-11.11±0.04	-10.93±0.03	-10.81±0.02	-10.75±0.01	-10.73±0.01	-10.72±0.01	-10.71±0.01
msnbc	-6.39±0.04	-6.25±0.02	-6.17±0.01	-6.15±0.01	-6.15±0.01	-6.15±0.01	-6.14±0.01
msweb	-10.31±0.04	-10.03±0.04	-9.80±0.01	-9.72±0.00	-9.69±0.00	-9.69±0.00	-9.68±0.00
nlcs	-6.08±0.00	-6.03±0.00	-6.00±0.00	-6.00±0.00	-6.00±0.00	-5.99±0.00	-5.99±0.00
plants	-14.72±0.16	-13.71±0.14	-12.99±0.02	-12.65±0.03	-12.54±0.03	-12.49±0.03	-12.45±0.02
pumbs	-39.41±0.89	-33.67±0.52	-30.01±0.10	-28.50±0.04	-28.05±0.05	-27.85±0.02	-27.67±0.03
tmovie	-51.95±0.26	-50.68±0.08	-49.59±0.13	-49.12±0.08	-48.87±0.08	-48.78±0.10	-48.69±0.09
tretail	-10.96±0.04	-10.90±0.02	-10.87±0.00	-10.85±0.00	-10.85±0.00	-10.85±0.00	-10.85±0.00

Table 8: Average $\text{cm}(\mathcal{S}_{\text{CLT}})$ test log-likelihoods across 5 random seeds. Higher is better.

Dataset	Mix-2 ⁷	Mix-2 ⁸	Mix-2 ⁹	Mix-2 ¹⁰	Mix-2 ¹¹	Mix-2 ¹²	Mix-2 ¹³
accidents	-31.00±0.15	-30.06±0.09	-29.28±0.05	-28.93±0.02	-28.79±0.01	-28.74±0.01	-28.69±0.01
ad	-16.67±0.39	-15.89±0.25	-15.27±0.08	-14.97±0.11	-14.85±0.11	-14.81±0.10	-14.76±0.10
baudio	-39.88±0.07	-39.51±0.08	-39.21±0.02	-39.08±0.02	-39.04±0.02	-39.03±0.02	-39.02±0.02
bbc	-249.01±0.94	-246.56±0.73	-244.75±0.51	-243.75±0.56	-243.27±0.54	-243.07±0.52	-242.83±0.55
bnetflix	-56.54±0.06	-56.01±0.07	-55.60±0.03	-55.42±0.02	-55.35±0.02	-55.34±0.02	-55.31±0.02
book	-34.29±0.10	-34.04±0.04	-33.90±0.03	-33.83±0.03	-33.79±0.03	-33.77±0.03	-33.75±0.03
c20ng	-151.59±0.45	-150.39±0.28	-149.28±0.17	-148.68±0.11	-148.41±0.09	-148.28±0.09	-148.17±0.09
cr52	-85.39±0.40	-83.82±0.24	-82.35±0.14	-81.70±0.09	-81.41±0.11	-81.30±0.09	-81.17±0.11
cwebkb	-150.73±0.28	-149.55±0.20	-148.59±0.21	-148.18±0.24	-147.94±0.25	-147.86±0.26	-147.77±0.26
dna	-86.79±0.25	-86.09±0.16	-85.49±0.09	-85.16±0.08	-85.01±0.07	-84.96±0.09	-84.91±0.09
jester	-52.55±0.05	-52.27±0.03	-52.06±0.02	-51.98±0.01	-51.95±0.01	-51.95±0.01	-51.94±0.01
kdd	-2.16±0.01	-2.14±0.00	-2.13±0.00	-2.12±0.00	-2.12±0.00	-2.12±0.00	-2.12±0.00
kosarek	-10.68±0.03	-10.63±0.02	-10.59±0.01	-10.57±0.01	-10.57±0.01	-10.56±0.01	-10.56±0.01
msnbc	-6.44±0.16	-6.22±0.10	-6.09±0.01	-6.07±0.00	-6.06±0.00	-6.06±0.00	-6.05±0.00
msweb	-9.89±0.05	-9.78±0.03	-9.67±0.02	-9.64±0.01	-9.63±0.01	-9.63±0.01	-9.62±0.01
nlts	-6.05±0.02	-6.03±0.02	-6.00±0.00	-6.00±0.00	-6.00±0.00	-6.00±0.00	-5.99±0.00
plants	-13.68±0.13	-12.98±0.07	-12.53±0.02	-12.35±0.01	-12.30±0.02	-12.28±0.01	-12.26±0.01
pumbs	-26.29±0.22	-25.22±0.22	-24.26±0.07	-23.92±0.02	-23.80±0.02	-23.76±0.03	-23.71±0.03
tmovie	-51.67±0.27	-50.59±0.16	-49.90±0.12	-49.56±0.01	-49.38±0.10	-49.29±0.11	-49.23±0.10
tretail	-10.84±0.01	-10.83±0.01	-10.82±0.01	-10.82±0.01	-10.82±0.01	-10.82±0.01	-10.82±0.01

Table 9: Latent Optimisation (LO) results for $\text{cm}(\mathcal{S}_{\text{CLT}})$. Integration points optimised for 150 epochs (with early stopping) using Adam with learning rate of 0.001.

Dataset	Mix-2 ⁷	Mix-2 ⁷ (LO)	Mix-2 ⁸	Mix-2 ⁸ (LO)	Mix-2 ⁹	Mix-2 ⁹ (LO)	Mix-2 ¹⁰	Mix-2 ¹⁰ (LO)
accidents	-31.00±0.15	-29.81±0.03	-30.06±0.09	-29.36±0.05	-29.28±0.05	-29.05±0.03	-28.93±0.02	-28.81±0.02
ad	-16.67±0.39	-15.08±0.17	-15.89±0.25	-14.73±0.13	-15.27±0.08	-14.51±0.11	-14.97±0.11	-14.42±0.09
baudio	-39.88±0.07	-39.45±0.04	-39.51±0.08	-39.25±0.03	-39.21±0.02	-39.11±0.02	-39.08±0.02	-39.04±0.02
bbc	-249.01±0.94	-245.57±0.75	-246.56±0.73	-244.03±0.74	-244.75±0.51	-243.25±0.59	-243.75±0.56	-242.79±0.58
bnetflix	-56.54±0.06	-56.02±0.03	-56.01±0.07	-55.69±0.02	-55.60±0.03	-55.48±0.02	-55.42±0.02	-55.36±0.02
book	-34.29±0.10	-33.79±0.07	-34.04±0.04	-33.69±0.08	-33.90±0.03	-33.61±0.06	-33.83±0.03	-33.55±0.02
c20ng	-151.59±0.45	-149.95±0.31	-150.39±0.28	-149.16±0.26	-149.28±0.17	-148.65±0.17	-148.68±0.11	-148.28±0.11
cr52	-85.39±0.40	-83.28±0.23	-83.82±0.24	-82.25±0.22	-82.35±0.14	-81.67±0.18	-81.70±0.09	-81.31±0.15
cwebkb	-150.73±0.28	-148.82±0.21	-149.55±0.20	-148.33±0.20	-148.59±0.21	-147.95±0.23	-148.18±0.24	-147.75±0.26
dna	-86.79±0.25	-85.64±0.24	-86.09±0.16	-85.03±0.13	-85.49±0.09	-84.78±0.12	-85.16±0.08	-84.58±0.10
jester	-52.55±0.05	-52.23±0.03	-52.27±0.03	-52.06±0.02	-52.06±0.02	-51.98±0.02	-51.98±0.01	-51.94±0.02
kdd	-2.16±0.01	-2.13±0.00	-2.14±0.00	-2.12±0.00	-2.13±0.00	-2.12±0.00	-2.12±0.00	-2.12±0.00
kosarek	-10.68±0.03	-10.60±0.01	-10.63±0.02	-10.58±0.01	-10.59±0.01	-10.56±0.01	-10.57±0.01	-10.55±0.01
msnbc	-6.44±0.16	-6.08±0.01	-6.22±0.10	-6.06±0.00	-6.09±0.01	-6.05±0.00	-6.07±0.00	-6.05±0.00
msweb	-9.89±0.05	-9.67±0.01	-9.78±0.03	-9.64±0.02	-9.67±0.02	-9.61±0.01	-9.64±0.01	-9.60±0.01
nlts	-6.05±0.02	-6.00±0.00	-6.03±0.02	-6.00±0.00	-6.00±0.00	-5.99±0.00	-6.00±0.00	-5.99±0.00
plants	-13.68±0.13	-12.76±0.04	-12.98±0.07	-12.50±0.02	-12.53±0.02	-12.34±0.02	-12.35±0.01	-12.27±0.01
pumbs	-26.29±0.22	-24.63±0.05	-25.22±0.22	-24.17±0.07	-24.26±0.07	-23.86±0.04	-23.92±0.02	-23.70±0.02
tmovie	-51.67±0.27	-50.31±0.18	-50.59±0.16	-49.79±0.23	-49.90±0.12	-49.40±0.12	-49.56±0.01	-49.29±0.12
tretail	-10.84±0.01	-10.82±0.01	-10.83±0.01	-10.81±0.01	-10.82±0.01	-10.81±0.01	-10.82±0.01	-10.81±0.01

Table 10: Results on 20 density estimation benchmarks. Average test-set log-likelihood of all baselines as reported on the respective papers: Strudel (Dang, Vergari, and Broeck 2020), LearnPSDD (Liang, Bekker, and Van den Broeck 2017), EinSumNet (Peharz et al. 2020a), LearnSPN (Gens and Pedro 2013), ID-SPN (Rooshenas and Lowd 2014), and RAT-SPN (Peharz et al. 2020b). Results for $\text{cm}(\mathcal{S}_F)$ and $\text{cm}(\mathcal{S}_{\text{CLT}})$ are computed with 2^{13} integration points. Higher is better.

Dataset	HCLT	EiNet	LearnSPN	ID-SPN	RAT-SPN	Strudel	LearnPSDD	$\text{cm}(\mathcal{S}_F)$	$\text{cm}(\mathcal{S}_{\text{CLT}})$
accidents	-26.78	-35.59	-40.50	-26.98	-35.48	-29.46	-28.29	-33.27	-28.69
ad	-16.04	-26.27	-19.73	-19.00	-48.47	-16.52	-20.13	-18.72	-14.76
baudio	-39.77	-39.87	-40.53	-39.79	-39.95	-42.26	-41.51	-39.02	-39.02
bbc	-250.07	-248.33	-250.68	-248.93	-252.13	-258.96	-260.24	-240.19	-242.83
bnetflix	-56.28	-56.54	-57.32	-56.36	-56.85	-58.68	-58.53	-55.49	-55.31
book	-33.84	-34.73	-35.88	-34.14	-34.68	-35.77	-36.06	-33.67	-33.75
c20ng	-151.92	-153.93	-155.92	-151.47	-152.06	-160.77	-160.43	-148.24	-148.17
cr52	-84.67	-87.36	-85.06	-83.35	-87.36	-92.38	-93.30	-81.52	-81.17
cwebkb	-153.18	-157.28	-158.20	-151.84	-157.53	-160.50	-161.42	-150.21	-147.77
dna	-79.33	-96.08	-82.52	-81.21	-97.23	-87.10	-83.02	-95.64	-84.91
jester	-52.45	-52.56	-75.98	-52.86	-52.97	-55.30	-54.63	-51.93	-51.94
kdd	-2.18	-2.18	-2.18	-2.13	-2.12	-2.17	-2.17	-2.13	-2.12
kosarek	-10.66	-11.02	-10.98	-10.60	-10.88	-10.98	-10.99	-10.70	-10.56
msnbc	-6.05	-6.11	-6.11	-6.04	-6.03	-6.05	-6.04	-6.14	-6.05
msweb	-9.90	-10.02	-10.25	-9.73	-10.11	-10.19	-9.93	-9.68	-9.62
nltes	-6.00	-6.01	-6.11	-6.02	-6.01	-6.06	-6.03	-5.99	-5.99
plants	-14.31	-13.67	-12.97	-12.54	-13.43	-13.72	-13.49	-12.45	-12.26
pumbs	-23.32	-31.95	-24.78	-22.40	-32.53	-25.28	-25.40	-27.67	-23.71
tmovie	-50.69	-51.70	-52.48	-51.51	-53.63	-59.47	-55.41	-48.69	-49.23
tretail	-10.84	-10.91	-11.04	-10.85	-10.91	-10.90	-10.92	-10.85	-10.82

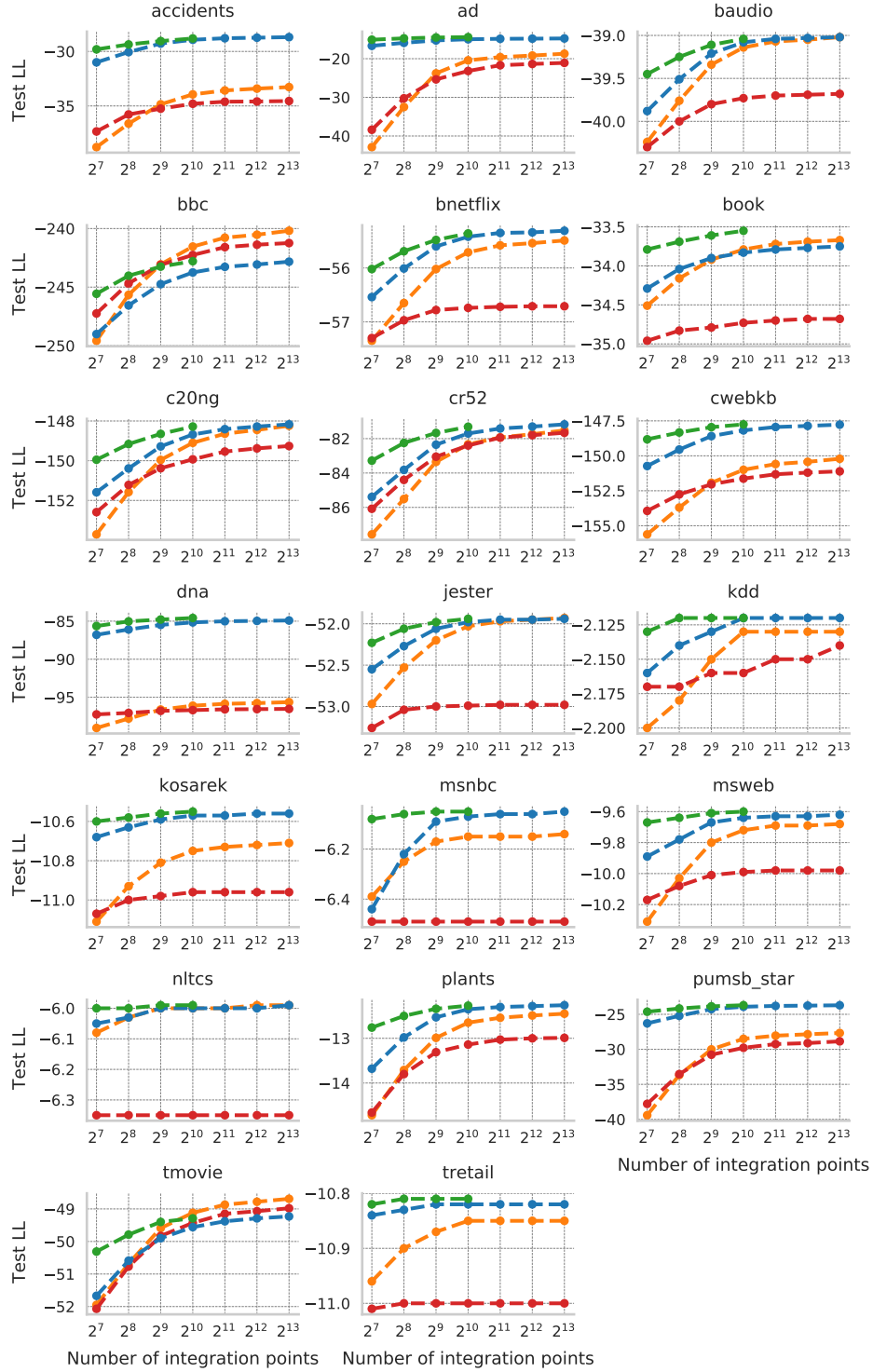


Figure 4: Test log-likelihood against number of integration points for $\text{cm}(\mathcal{S}_F)$ (orange), $\text{cm}(\mathcal{S}_{\text{CLT}})$ (blue), $\text{LO}(\text{cm}(\mathcal{S}_{\text{CLT}}))$ (green) and $\text{cm}(\mathcal{S}_F^{\text{VAE}})$ (red). Results are averaged over 5 random seeds.

F Demonstration of Tractable Queries

F.1 Training with missing data

Our models support efficient marginalisation out-of-the-box both at training and test time, like any other Probabilistic Circuit (PC). More precisely, for any partition of the domain variables into observed \mathbf{X}_o and not observed variables \mathbf{X}_{-o} , one can compute $p(\mathbf{X}_o) = \int_{\mathbf{x}_{-o}} p(\mathbf{X}_o, \mathbf{x}_{-o}) d\mathbf{x}_{-o}$, with the same computational complexity of computing $p(\mathbf{X})$. This is formally demonstrated for Sum-Product Networks (Peharz et al. 2015); a class of PCs to which our approximate model $\sum_{i=1}^N w(\mathbf{z}_i) p(\mathbf{x} | \phi(\mathbf{z}_i))$ belongs to. In a nutshell, marginalisation in PCs boils down to evaluating marginals at the leaves, which is often simple to compute (e.g. with univariate leaves). That is the same for continuous mixtures, where inference is performed via the approximate model above; itself a PC supporting efficient exact marginalisation. That means, numerical integration can approximate any marginal query in continuous mixtures in the exact same principled manner, without requiring imputation or ad-hoc techniques to handle missing values. We illustrate this by showing samples from a $\text{cm}(\mathcal{S}_F)$ trained only with incomplete binary MNIST samples, as depicted in Figure 5. At training time, we omit blocks of pixels from each image completely at random, meaning the model never observes a complete digit. Nonetheless, the model generates complete and reasonable digits, indicating proper marginalisation of the missing pixels at training time.



Figure 5: Illustration of the ability of $\text{cm}(\mathcal{S}_F)$ to handle missing data via marginalisation. On top we have binary MNIST training images with blocks of pixels omitted at random. We display the training images in colour to distinguish pixel values from non-observed pixels (depicted in white). On the bottom, we have samples (continuous Bernoulli) from a $\text{cm}(\mathcal{S}_F)$ trained on incomplete binary MNIST images, like the ones shown above. The models always generate complete digits, despite never observing one during training.

F.2 Inpainting

Our models also support efficient Most Probable Explanations (MPE) queries. This property also stems directly from the underlying PC in the approximate model $\sum_{i=1}^N w(\mathbf{z}_i) p(\mathbf{x} | \phi(\mathbf{z}_i))$. In Figure 6, we demonstrate an application of this type of query via inpainting with a $\text{cm}(\mathcal{S}_F)$ model on binary MNIST. To compute an MPE for the images

in Figure 6, we first compile the model to a discrete mixture with 2^{14} integration points and evaluate the approximate model on the incomplete images (possible thanks to efficient marginalisation in PCs as discussed above). This allows us to perform a simple (approximate) posterior inference by selecting, for each image, the component (integration point) that is the most likely to have generated it. Finally, we sample from these individual components to produce the final reconstruction. Albeit simple, this MPE procedure produces good reconstructions as shown in Figure 6. Note that, for the results in Figure 6, we use the same set of integration points to run MPE on each and every image. That means, the results demonstrated here are equivalent regardless of the interpretation of the model: numerical integration on the continuous mixture, or exact inference on a compiled PC.

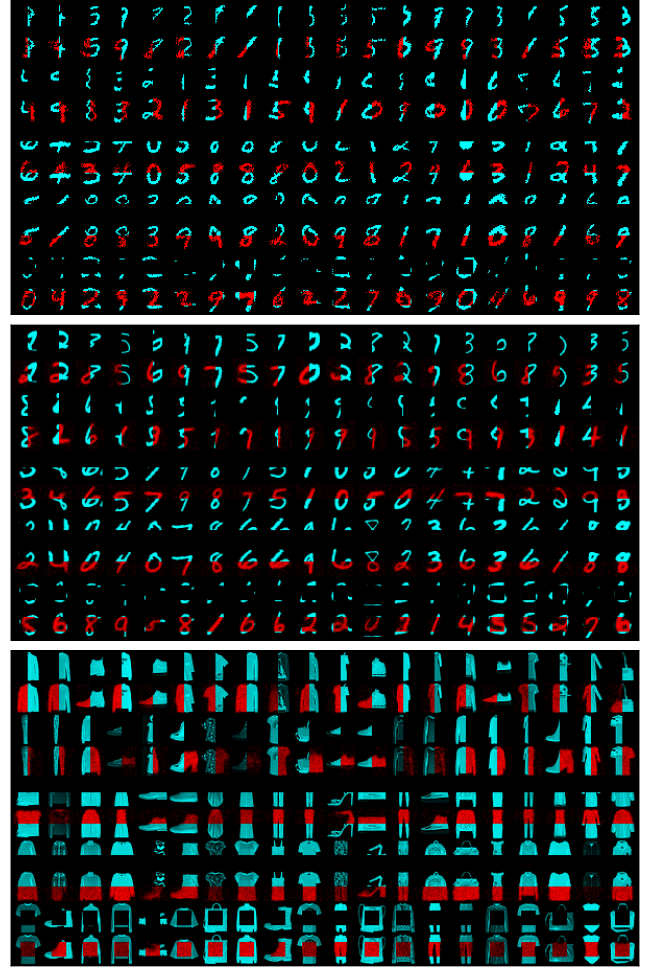


Figure 6: Inpainting results on binary MNIST (top), MNIST (middle) and Fashion-MNIST (bottom) obtained with $\text{cm}(\mathcal{S}_F)$. In alternating rows, we have first the original image with a missing part, and below the reconstructed image output by $\text{cm}(\mathcal{S}_F)$. Pixels from the original (reconstructed) images are depicted in blue (red).

G Monte Carlo (MC) vs Randomised Quasi Monte Carlo (RQMC)

In practice, Randomised Quasi Monte Carlo (RQMC) can be seen as a variance reduction method (l’Ecuyer 2016), which often translates in faster convergence of learning algorithms (Buchholz, Wenzel, and Mandt 2018). We also have observed RQMC to improve convergence in our use cases, and thus have used RQMC in all our experiments. To illustrate this, we compare the training of $\text{cm}(\mathcal{S}_F)$ on binary-MNIST using MC and RQMC. In Figure 7, it is clear that RQMC facilitates learning and improves the overall solution by a small but non-negligible amount.

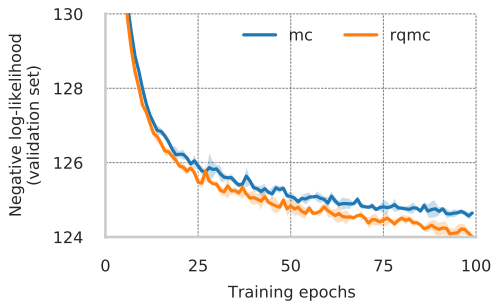


Figure 7: Log-likelihood on validation set against number of training epochs for $\text{cm}(\mathcal{S}_F)$ trained on binary-MNIST with MC (blue) and RQMC (orange). We use 2^{10} integration points in both cases and plot one standard deviation confidence bands computed with 5 different random seeds.